

# Dark Energy and Dark Matter Haloes

Michael Kuhlen<sup>1</sup>, Louis E. Strigari<sup>2</sup>, Andrew R. Zentner<sup>3,4</sup>, James S. Bullock<sup>5\*</sup>  
and Joel R. Primack<sup>6</sup>

<sup>1</sup>*Department of Astronomy and Astrophysics, University of California at Santa Cruz, 1156 High Street, Santa Cruz, CA 95064*

<sup>2</sup>*Department of Physics, The Ohio State University, 174 W. 18th Avenue, Columbus, OH 43210*

<sup>3</sup>*Center for Cosmological Physics, The University of Chicago, 5640 S. Ellis Avenue, Chicago, IL 60637*

<sup>4</sup>*Department of Astronomy and Astrophysics, The University of Chicago, 5640 S. Ellis Avenue, Chicago, IL 60637*

<sup>5</sup>*Harvard-Smithsonian Center for Astrophysics, 60 Garden Street, Cambridge, MA 02138*

<sup>6</sup>*Physics Department, University of California at Santa Cruz, 1156 High Street, CA 95064*

Submitted 2004 April 05

## ABSTRACT

We investigate the effect of dark energy on the density profiles of dark matter haloes with a suite of cosmological N-body simulations and use our results to test analytic models. We consider constant equation of state models, and allow both  $w \geq -1$  and  $w < -1$ . Using five simulations with  $w$  ranging from  $-1.5$  to  $-0.5$ , and with more than  $\sim 1600$  well-resolved haloes each, we show that the halo concentration model of Bullock et al. (2001) accurately predicts the median concentrations of haloes over the range of  $w$ , halo masses, and redshifts that we are capable of probing. We find that the Bullock et al. (2001) model works best when halo masses and concentrations are defined relative to an outer radius set by a cosmology-dependent virial overdensity. For a fixed power spectrum normalization and fixed-mass haloes, larger values of  $w$  lead to higher concentrations and higher halo central densities, both because collapse occurs earlier and because haloes have higher virial densities. While precise predictions of halo densities are quite sensitive to various uncertainties, we make broad comparisons to galaxy rotation curve data. At fixed power spectrum normalization (fixed  $\sigma_8$ ),  $w > -1$  quintessence models seem to exacerbate the central density problem relative to the standard  $w = -1$  model. For example, models with  $w \simeq -0.5$  seem disfavored by the data, which can be matched only by allowing extremely low normalizations,  $\sigma_8 \lesssim 0.6$ . Meanwhile  $w < -1$  models help to reduce the apparent discrepancy. We confirm that the Jenkins et al. (2001) halo mass function provides an excellent approximation to the abundance of haloes in our simulations and extend its region of validity to include models with  $w < -1$ .

**Key words:** cosmology: theory – dark matter – large-scale structure of universe – methods: N-body simulations

## 1 INTRODUCTION

In the prevailing model of galaxy formation, galaxies assemble and evolve in the potential wells established by gravitationally bound haloes of cold and collisionless dark matter (CDM). Except for some possible difficulties on small scales, the CDM model is remarkably successful in explaining a large number of observations. However, this success requires an additional “dark energy” component, that drives an accelerated cosmic expansion, to be added to the universal energy budget. While the presence of dark energy is firmly established observationally, measuring its equation of state

as well as developing a theoretical understanding of the nature of the dark energy are two of the biggest outstanding problems in cosmology today. Dark energy not only affects the large-scale evolution of the Universe, but also the collapse histories and density structures of dark matter haloes. Understanding the precise nature of these effects is important for studies that aim to quantify the nature of dark energy using strong (e.g., Sarbu, Rusin, & Ma 2001; Huterer & Ma 2004; Kuhlen, Keeton, & Madau 2004) and weak (e.g. Hu & Jain 2003; Bartelmann et al. 2002) gravitational lensing. Changing the dark energy model should similarly change expectations for galaxy rotation curves, and could affect one of the main small-scale problems facing CDM – the central density problem (e.g., Zentner & Bullock 2002; McGaugh, Barker, & de Blok 2003, and references therein).

\* Hubble Fellow

In the present paper, we use a suite of N-body simulations to study how halo density profiles change as a function of dark energy equation of state, discuss our results in the context of analytic models, and discuss the observational implications of dark energy on galaxy scales.

The existence of some form of dark energy is supported by a preponderance of data. Taken together, observations of the magnitude-redshift relation of type Ia supernovae (SNIa; Perlmutter et al. 1999; Riess et al. 2001; Knop et al. 2003; Barris et al. 2003), the power spectrum of cosmic microwave background (CMB) anisotropy (Spergel et al. 2003; Tegmark et al. 2003a), the power spectrum of galaxy clustering (Dodelson et al. 2003; Tegmark et al. 2003b), and the luminosity function and baryon fraction of clusters (Allen et al. 2003) provide nearly unimpeachable evidence for the existence of dark energy. The most common supposition is that the dark energy takes the form of a cosmological constant or vacuum energy. In this case, the energy density  $\rho$ , and pressure  $p$ , are related through  $p = -\rho$ . An attractive alternative candidate for the dark energy is the potential energy of a slowly-varying scalar field  $\phi$ , or “quintessence” (e.g., Ratra & Peebles 1988; Caldwell, Davé, & Steinhardt 1998).

A convenient parametrization of the dark energy is through an equation of state  $w \equiv p_\phi/\rho_\phi$  relating its energy density and pressure. In general, the equation of state parameter  $w$  is time-varying, but it is useful to model quintessence with a constant equation of state parameter because current observational data sets have limited power to distinguish between a time-varying and constant equation of state (e.g., Kujat et al. 2002). Useful limits on the equation of state for the dark energy, assuming that it remains constant in time, come from SNIa studies,  $-1.67 < w < -0.62$  ( $2\sigma$ ; Knop et al. 2003), and can be refined by combining SNIa data with CMB anisotropy and galaxy clustering statistics yielding  $-1.33 < w < -0.79$  at  $2\sigma$  (Tegmark et al. 2003b). For our simulations, we adopt an empirical view and study five models with constant  $w$ , that span a comparably large range of parameter space:  $w = -1.5, -1.25, -1.0, -0.75, -0.5$ .

Our theoretical understanding of halo profiles has improved recently largely through numerical simulations, performed in the context of  $\Lambda$ CDM plus cosmological constant ( $\Lambda$ CDM) or standard CDM (SCDM, i.e.  $\Omega_M = 1$ ,  $\Omega_Q = 0$ ) cosmologies (Navarro, Frenk, & White, 1995, 1996, 1997, hereafter NFW; Kravtsov, Klypin, & Khokhlov 1997; Ghigna et al. 1998; Jing 2000; Bullock et al. 2001; Eke, Navarro, & Steinmetz 2001; Wechsler et al. 2002, hereafter W02; Zhao et al. 2003; Hayashi et al. 2003; Navarro et al. 2003; for a review, see Primack 2003). It is generally understood that the final density profiles of haloes are linked closely to their formation histories. Halo central densities are set during an early, rapid-accretion phase, and tend to be proportional to the density of haloes in the Universe at the time of this rapid collapse (W02; Zhao et al. 2003; Tasitomi et al. 2003). Larger values of  $w$  lead to earlier collapse times and also to more rapid collapse of overdensities, thus we expect haloes with higher relative central densities and higher virial densities (see our discussions in § 2 and § 3). In §§ 4-6 we quantify these effects and test the expected scalings. We verify that the analytic technique of Bullock et al. (2001, B01) for predicting halo concentrations works well

when applied directly to constant  $w$  cosmologies, implying that it is fairly generally applicable.

A related issue is the effect of dark energy on the halo mass function. Although it is not directly observable, theoretical insight into the expected halo mass function is attainable through current N-body simulations. The effects of dark energy on halo mass functions have been investigated by Bartelmann, Perota, & Baccigalupi (2003), Linder & Jenkins (2003), Klypin et al. (2003), Macciò et al. (2003), and Lokas, Bode, & Hoffman (2003) and the accurate prediction of halo mass functions as well as accretion histories and density structures over a large range of redshifts is necessary in order to take full advantage of the ability of upcoming cluster surveys, such as the Sunyaev-Zeldovich Array (<http://astro.uchicago.edu/sza/>), to constrain the dark energy equation of state (see Carlstrom, Holder, & Reese 2001 for a review). There appears to be general agreement that halo mass functions can be approximated accurately by the “universal” mass function of Jenkins et al. (2001, hereafter J01) even in models with dark energy. In § 5.1, we confirm the results of previous studies of quintessence cosmologies with  $w > -1$ , and extend this agreement to models with  $w < -1$ .

Klypin et al. (2003) and Dolag et al. (2003) have performed previous numerical studies of CDM haloes in quintessence cosmologies. Where our study overlaps with these, our results are generally in agreement. This study extends, complements, and improves upon previous studies in several ways. We have investigated the effects of normalizing the power spectrum using clusters vs. CMB, which yield quite different results. We have assembled large catalogues of haloes, with masses and concentrations for more than 1600 haloes with more than 100 particles each in each simulation. With this large number of haloes we are able to measure the distribution of concentrations at fixed mass and test the predictions of the B01 model for both the mean relation between concentration and mass and the halo-to-halo scatter. We also extend the range of quintessence parameter space probed by simulations by exploring two models with  $w < -1$ .

The format of this paper is as follows. After a brief review of the basics of structure formation in models with dark energy in § 2, we go on in § 3 to describe modifications to the B01 model for halo concentrations in quintessence cosmologies. In § 4, we describe the set of numerical simulations that we performed. In § 5, we present the mass functions and concentrations of CDM haloes in these simulations and compare them to the results of the analytic B01 model. In § 6, we briefly discuss the central density problem of CDM in light of our results. In § 7, we present a summary of our findings, highlight improvements and differences to previous studies, and discuss the implications of this work. Throughout this paper, we assume a flat universe with present matter density relative to critical of  $\Omega_M = 0.3$ , and Hubble parameter  $h = 0.7$ . The quintessence energy density is then  $\Omega_Q = 1 - \Omega_M = 0.7$ . We refer to a model with a cosmological constant ( $w = -1$ ) as  $\Lambda$ CDM. We use the terms “quintessence” and “QCDM” to refer to all models which have  $w \neq -1$ .

## 2 STRUCTURE FORMATION IN QUINTESSENCE COSMOLOGIES

In this Section, we present a brief overview of the growth of structure in quintessence cosmologies. In §2.1, we introduce the basic results of cosmological perturbation theory with quintessence and discuss our computations of the matter power spectrum. We briefly discuss the normalization of the power spectrum in §2.2. A convenient way to define the mass and radius of a dark matter halo is through a mean overdensity  $\Delta_{\text{vir}}$ , relative to the background density (see §3.1). The idea is to choose  $\Delta_{\text{vir}}$  so as to delineate the boundary between virialized and in-falling material. The equivalent linear overdensity at collapse  $\delta_c$ , is a quantity that is used to delineate the mass scale of objects that are forming at a particular redshift. Often, these overdensity criteria are chosen with reference to the evolution of a spherical tophat overdensity. In §2.3, we discuss the spherical tophat model in quintessence cosmologies.

We explore both conventional quintessence models with  $w \geq -1$  and, adopting an empirical approach, we pursue models with  $w < -1$ . Requiring the kinetic energy of the quintessence to be positive imposes the condition  $w \geq -1$  on the quintessence equation of state. When  $w \geq -1$  and constant, all computations can be performed knowing only the value of  $w$  by assuming that the scalar field Lagrangian has a canonical kinetic term. To explore the parameter space  $w < -1$  self-consistently, we must choose a particular model for scalar field dynamics and one simple possibility is a Lagrangian with a non-canonical kinetic term that differs from the canonical case by a negative sign. Explicitly, we adopt the “phantom energy” Lagrangian for the field,  $\phi$ :  $\mathcal{L} = -\partial_\mu\phi\partial^\mu\phi - V(\phi)$  (Caldwell 2002; Carroll, Hoffmann, & Trodden 2003; Cline, Jeon, & Moore 2003). Having made this choice, we can express the derivatives of the potential completely in terms of  $w$  (Dave, Caldwell, & Steinhardt 2002).

### 2.1 Cosmological Perturbations

Here we consider linear perturbations to the CDM density field,  $\delta(\vec{x}) \equiv \delta\rho(\vec{x})/\rho_b$ , with  $\rho_b$  the mean density of dark matter in the universe. The linear evolution of  $\delta(\vec{x})$  follows from solving the linearized Einstein-Boltzmann equations (e.g., Ma & Bertschinger 1995). We perform our calculations in the synchronous gauge with a modified version of the publicly-available Einstein-Boltzmann code CMBfast by Seljak & Zaldarriaga (1996). We assume a scale-invariant spectrum of adiabatic primordial density fluctuations and a baryon density  $\Omega_B h^2 = 0.02$ .

The linear equation for fluctuations in the quintessence field in Fourier space is

$$\ddot{\delta\phi} + 3H\dot{\delta\phi} + (k^2/a^2 \pm V_{,\phi\phi})\delta\phi = \dot{\delta}_k[(1+w_Q)\rho_\phi]^{1/2}, \quad (1)$$

where  $V_{,\phi\phi} \equiv \partial^2 V/\partial\phi^2$ ,  $\rho_\phi$  is the mean energy density in the quintessence field, and the plus (minus) signs correspond to fields with positive (negative) kinetic energy. Here the dots represent derivatives with respect to cosmological proper time  $t$ , and  $\delta_k$  is the linear CDM fluctuation in Fourier space. The power spectrum of linear density perturbations is defined as  $P(k) \equiv \langle |\delta_k|^2 \rangle$ . The CDM transfer functions for our scale-invariant primordial spectrum are defined from

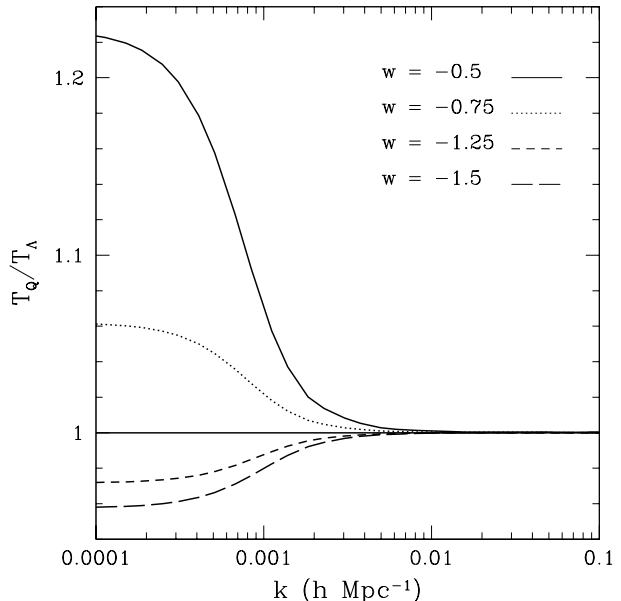


**Figure 1.** The ratio of  $z = 0$  quintessence transfer functions to  $\Lambda$ CDM for different models. The transfer functions are similar for wavenumbers  $k \gtrsim 0.01 h \text{ Mpc}^{-1}$ . The different equation of state parameters are shown in the legend.

$$P(k, z) = A_Q k T^2(k, z) \frac{D^2(z)}{D^2(0)}, \quad (2)$$

where  $A_Q$  is the normalization and  $D(z) \equiv \delta(z)/\delta(0)$  is the linear growth factor. On scales larger than the Compton wavenumber,  $k_Q \sim \sqrt{V_{,\phi\phi}}$ ,  $\delta\phi$  can grow and source the evolution of  $\delta_k$ . Contrarily, on small scales  $k \lesssim k_Q$ , perturbations in the quintessence field decay, so the  $Q$ CDM transfer functions have the same form as those of standard  $\Lambda$ CDM, while on scales  $k \lesssim k_Q$ , the transfer functions reflect the clustering of  $\phi$  (Ma, Caldwell, Bode, & Wang 1999). Figure 1 shows the ratio of the CDM transfer functions with quintessence,  $T_Q$ , to the transfer function in the corresponding  $\Lambda$ CDM model ( $w = -1$ ),  $T_\Lambda$ , at  $z = 0$ . For  $k \lesssim k_Q$  and  $w \geq -1$ , perturbations in the quintessence field,  $\delta\rho_\phi - 3\delta p_\phi$ , source the growth of  $\delta_k$ . For  $w \leq -1$ , the source term from the quintessence field changes sign, resulting in a relative decrease in  $\delta_k$ .

### 2.2 Power Spectrum Normalization

One of the most important parameters determining the scale radii of halo density profiles is the normalization of the matter power spectrum on small scales. In our N-body experiments, we choose to normalize each  $w$  model with similar values of  $\sigma_8$ , set by cluster abundance estimates. We do so because the abundance of clusters is a more direct probe of the amount of power on the scales that are relevant to galaxy formation than the CMB anisotropy measurements and in order to isolate the differences that arise because of variations in the expansion rate in models with different values of  $w$ .

We normalize the power spectrum to the abundance of massive clusters using x-ray flux and temperature measurements from the cores of clusters of galaxies, and the

corresponding conversion to cluster mass from the mass-temperature ( $M$ - $T$ ) relation. With all other cosmological parameters fixed, a comparison of the observed mass function to the predicted mass functions from N-body simulations (J01) determines the normalization parameter  $\sigma_8$ . The quintessence field is smooth on scales much smaller than the horizon size, thus the values of  $\sigma_8$  derived from  $z = 0$  cluster measurements are rather insensitive to  $w$ .

The largest source of error in the determination of  $\sigma_8$  from clusters is the uncertainty in the normalization of the  $M$ - $T$  relation. Simulations consistently predict an  $M$ - $T$  relation that is a factor of  $\sim 2$  greater than the one observed from x-ray temperature data (e.g., Seljak 2002 and references therein). For  $\Lambda$ CDM and  $\Omega_M = 0.3$ , our current understanding of the  $M$ - $T$  relation places  $\sigma_8$  very broadly in the range  $0.65 \lesssim \sigma_8 \lesssim 1.1$  (Pierpaoli, Scott, & White 2001; Reiprich & Böhringer 2002; Pierpaoli et al. 2003). Using the HIFLUGCS cluster mass function (Reiprich & Böhringer 2002), we find for  $\Omega_M = 0.3$ ,  $\sigma_8 \simeq 0.74$ , nearly independently of  $w$  (Kuhlen, Keeton, & Madau 2004). We normalize the power spectra to  $\sigma_8 = 0.742, 0.740, 0.738, 0.736, 0.734$  for  $w = -1.5, -1.25, -1.0, -0.75, -0.50$  respectively. In principle, the value of  $\sigma_8$  as determined from clusters is degenerate with  $\Omega_M$  (e.g. Schuecker et al. 2003), indeed the global best fit to the HIFLUGUS sample is  $\Omega_M \simeq 0.12$ ,  $\sigma_8 \simeq 0.96$  in a  $\Lambda$ CDM cosmology; however, we adopt values of  $\sigma_8$  that best fit the data given our choice of  $\Omega_M = 0.3$ .

While we have chosen to normalize our numerical simulations using the cluster abundance, this normalization is fairly uncertain. In the interest of completeness, we remark that not all of these model normalizations are consistent with  $n = 1$  normalization to CMB anisotropy (even modulo uncertainties in the reionization epoch). In the simplest case, with all other cosmological parameters held fixed, the value of  $w$  affects the CMB-derived  $\sigma_8$  normalization primarily through the late-time integrated Sachs-Wolfe (ISW) effect (see Hu & Sugiyama 1995). For universes with  $w \geq -1$ , the quintessence energy density becomes comparable to that of CDM at earlier epochs relative to  $\Lambda$ CDM, resulting in greater variation in the gravitational potentials along lines of sight to the surface of last scattering. For lower values of  $w$ , the ISW effect is not as prominent because quintessence becomes dynamically important only at more and more recent epochs. In Figure 2, we show the value of  $\sigma_8$  implied by the CMB normalization as a function of the equation of state parameter  $w$ . As we stated above, the decrease in  $\sigma_8$  is due to the increased importance of the ISW effect as  $w$  increases.

Care must be taken when setting the CMB normalization. First, we note that when we performed our N-body experiments we fixed the parameter  $\Omega_M = 0.3$  for all models rather than allowing  $\Omega_M$  to vary along the  $\Omega_M$ - $w$  degeneracy in the angular diameter distance. Our most extreme models are currently disfavored by the present observational data (e.g., Tegmark et al. 2003; Knop et al. 2003), but as our intent is to address the effect of quintessence on structure and halo formation, we do not consider this to be a serious deficiency. In principle, the WMAP (Spergel et al. 2003) result of high optical depth to the last scattering surface  $\tau$ , has made the determination of  $\sigma_8$  from the CMB less robust, as the scattering off of free electrons damps anisotropies on scales that are sub-horizon at the epoch of reionization,

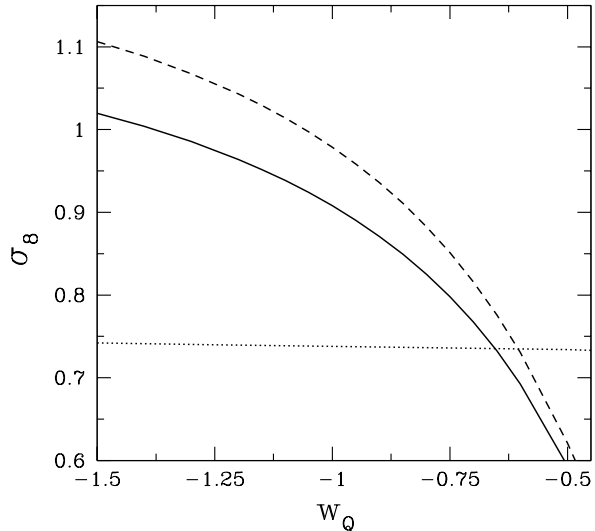


**Figure 2.** The power spectrum normalization  $\sigma_8$ , implied by CMB anisotropy as a function of  $w$ . The solid line shows the values of  $\sigma_8$  that we obtain by assuming the optical depth to the last scattering surface  $\tau = 0$ . The dashed line shows the values of  $\sigma_8$  implied by adopting  $\tau = 0.17$ . The dotted line shows the values of  $\sigma_8$  that we infer from the abundance of massive x-ray clusters.

thereby introducing a degeneracy between  $\tau$  and  $\sigma_8$ . The dashed line in Figure 2 shows the CMB-normalized  $\sigma_8$  as a function of  $w$  implied by adopting an optical depth to the last scattering surface of  $\tau = 0.17$ , in line with the WMAP expectations.<sup>1</sup> We return to a discussion of the relative importance of  $\sigma_8$  and  $w$  in §§ 6-7.

### 2.3 The Spherical Collapse Approximation

A common convention is to define the virial mass and radius of a dark matter halo by demanding that the mean density within the virial radius of the halo be a factor  $\Delta_{\text{vir}}$  times larger than the background density,  $\rho_b$ . Thus the virial mass and radius of a halo are related by

$$M_{\text{vir}} = \frac{4\pi}{3} \Delta_{\text{vir}} \rho_b R_{\text{vir}}^3. \quad (3)$$

In addition, the equivalent linear overdensity at collapse  $\delta_c(z)$  is often used to determine the mass scale that is typically collapsing at a given epoch. Both of these quantities are usually estimated using the approximation of spherical tophat collapse (e.g., Lacey & Cole 1993). In this section, we summarize the previous results for spherical collapse in quintessence cosmologies (Mainini et al. 2003; Mota & van

<sup>1</sup> Note that a high optical depth to reionization appears to be difficult to reconcile with low values of  $\sigma_8 \lesssim 0.75$  (e.g., Somerville, Bullock, & Livio 2003), though the CMB-derived  $\tau$  is very uncertain and is somewhat degenerate with the tilt of the power spectrum, so tilted models with low  $\sigma_8$  may still be viable. This issue will likely be settled with future CMB data and analysis.

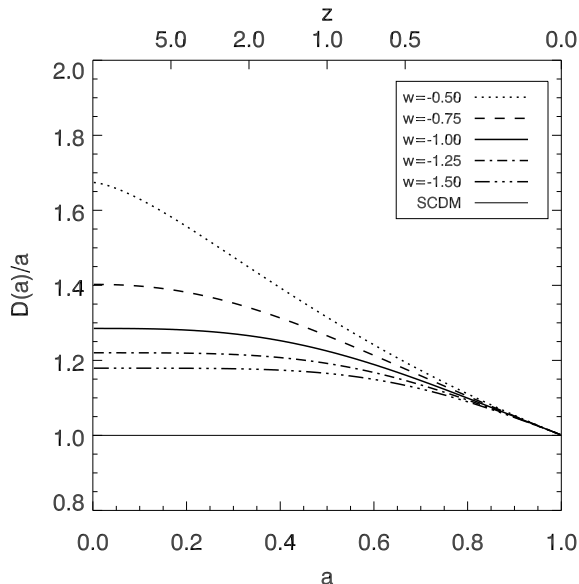


**Figure 3.** Ratio of the growth factor to the SCDM growth factor ( $D_{\text{SCDM}}(a) = a$ ) as a function of scalefactor for different values of  $w$ . The growth factor is normalized to unity today ( $D(a=1) = 1$ ). Linetypes are shown in the legend.

de Bruck 2004), and discuss the implications for  $w < -1$  cosmologies.

The evolution of linear overdensities on scales much smaller than those on which the quintessence field spatially clusters is

$$\ddot{\delta} + 2H(a)\dot{\delta} \simeq \frac{3}{2}H_0\Omega_M a^{-3}. \quad (4)$$

Solving this equation gives the growth factor for linear perturbations. Figure 3 shows the linear growth factor in five different quintessence models, normalized to the growth factor in an  $\Omega_M = 1$ , SCDM cosmology in which  $D(a) \propto a$ . Models with  $w \geq -1$  have been well-studied, with such models showing more relative growth at higher redshifts. For models with  $w \leq -1$ , figure 3 shows how the trend towards more relative growth at lower redshifts continues for  $w < -1$ .

To determine the non-linear growth of an object which has decoupled from the expanding universe and virialized, we follow Wang & Steinhardt (1998) and Weinberg & Kamionkowski (2003). We use the spherical collapse approximation to determine the non-linear overdensity of a halo,  $\Delta_{\text{vir}}(z)$ , as a function of  $z$ . In this model, an overdensity defined by  $\Delta_{\text{vir}}(z)$  collapses at the time  $t_{\text{coll}}$ , when the radius of the overdense region approaches zero. However, the actual, final radius of the collapsed object is finite and can be computed using the virial theorem. We compute the equivalent linear overdensity at collapse by evolving the linearized equation of motion, Eq. (4), until the time  $t_{\text{coll}}$ , determined from the non-linear evolution of the overdensity. In the  $\Lambda$ CDM cosmology, the well-known results for the linear and non-linear overdensities at collapse are  $\delta_c(z=0) \simeq 1.67$  and  $\Delta_{\text{vir}} \simeq 337$ , and vary with redshift.

Figure 4 shows our results for the equivalent linear overdensity at collapse  $\delta_c(z)$ , and the non-linear overdensity at

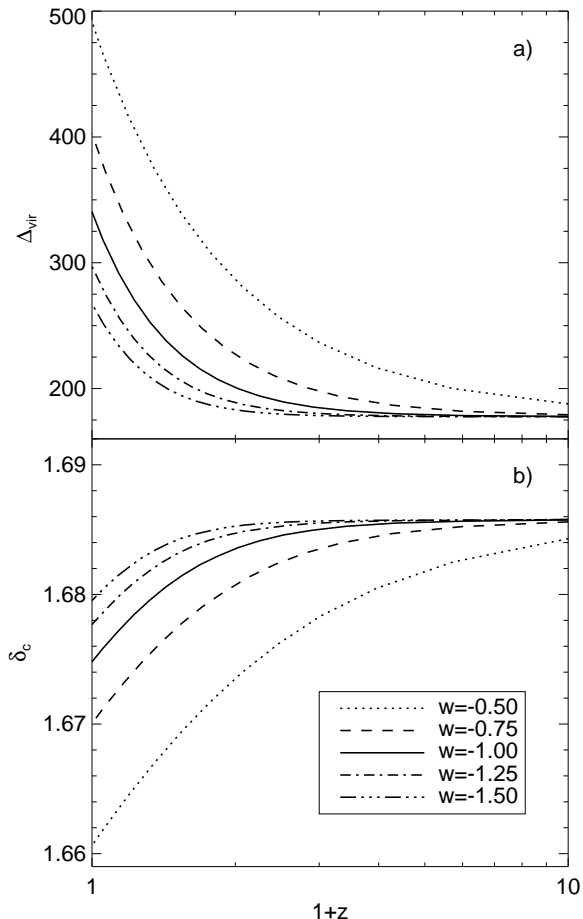


**Figure 4.** The non-linear and linear overdensities at collapse in quintessence cosmologies. In panel (a), we exhibit the non-linear overdensity at collapse  $\Delta_{\text{vir}}(z)$  for 5 different quintessence models that we explore in this paper ( $\Omega_M = 0.3$ ). The different values of the quintessence equation of state parameter  $w$ , are shown in the legend. The increase in  $\Delta_{\text{vir}}(z)$  for larger  $w$  results primarily from later collapse redshifts. In panel (b), we show the equivalent linear overdensity at collapse  $\delta_c(z)$ , as a function of redshift for the same quintessence models.

collapse  $\Delta_{\text{vir}}(z)$ , as a function of redshift in quintessence cosmologies. The trend in  $\delta_c(z)$  reflects the fact that overdensities grow more slowly in higher- $w$  models. We can understand the behavior of  $\Delta_{\text{vir}}(w, z)$  by noting that overdensities in models with larger  $w$  take longer to collapse at late times. Consider, for example, two haloes, one in a  $w = -1$  cosmology, and another in a  $w > -1$  cosmology, both of which are just virializing at some redshift  $z$ . Very roughly speaking, the  $w > -1$  halo will have had a turn-around time at a higher redshift than the  $w = -1$  halo, and its virial density will be higher to reflect this. Conversely  $w < -1$  models will have more recent turn-around times and smaller virial overdensities. We find that an accurate fitting function, including the regime  $w < -1$ , can be obtained from a slight

modification to the formula already proposed by Weinberg & Kamionkowski (2003) for  $w > -1$ ,

$$\Delta_{\text{vir}}(z) = 18\pi^2 [1 + a\Theta^b(z)], \quad (5)$$

where  $\Theta(z) \equiv \Omega_M^{-1}(z) - 1$ , and with  $a = 0.432 - 2.001(|w|^{0.234} - 1)$  and  $b = 0.929 - 0.222(|w|^{0.727} - 1)$ . We find this formula to be accurate to better than 2% for  $0.1 \leq \Omega_M \leq 1$  and  $-0.5 \leq w \leq -1.5$ .

### 3 ANALYTIC MODEL FOR HALO CONCENTRATIONS

#### 3.1 Main Ingredients

It is commonly agreed that the spherically-averaged density profiles of dark matter haloes can be described fairly well by a generalized NFW profile on scales that are resolved in state-of-the-art N-body simulations:

$$\rho_{\text{halo}}(r) = \frac{\rho_s}{(r/r_s)^\alpha (1 - r/r_s)^{3-\alpha}}, \quad (6)$$

where  $\alpha$  describes the slope of the inner density profile at  $r < r_s$ . The value of  $\alpha$  that most closely represents the results of N-body simulations is still debated, with acceptable values between  $-0.7$  and  $-1.5$ . An additional complexity is that recent studies indicate that haloes exhibit a range of inner slopes (Klypin et al. 2001; Tasitsiomi et al. 2003; Navarro et al. 2003). In the following, we adopt  $\alpha = -1$ , corresponding to the standard NFW profile. In this paper, we are concerned with the concentration parameter  $c_{\text{vir}}$ , which is quite insensitive to the exact value of  $\alpha$  (see below).

The two parameters of the NFW profile are  $r_s$  and  $\rho_s$ , with  $r_s$  the radius at which the logarithmic density slope becomes equal to  $-2$ . The concentration of the halo is defined as the ratio of its virial radius to the scale radius of the NFW profile,

$$c_{\text{vir}} = \frac{R_{\text{vir}}}{r_s}. \quad (7)$$

With these definitions, the halo virial mass is related to the NFW parameters by

$$M_{\text{vir}} = 4\pi\rho_s r_s^3 \left[ \ln(1 + c_{\text{vir}}) - \frac{c_{\text{vir}}}{1 + c_{\text{vir}}} \right], \quad (8)$$

so the halo density profile is completely determined by  $M_{\text{vir}}$  and  $c_{\text{vir}}$ .

Numerical simulations have revealed a correlation between  $M_{\text{vir}}$  and  $c_{\text{vir}}$ , with halo concentrations log-normally distributed around the median relation. Several simple models have been developed to explain this correlation (NFW; B01; Eke, Navarro, & Steinmetz 2001). Here we focus on the B01 model and test the accuracy with which it predicts the observed relation between halo mass and concentration in simulations with  $w \neq -1$ .

The B01 model assumes that a halo's central density and concentration are set by the density of the universe at a characteristic formation epoch. This formation epoch qualitatively tracks the characteristic collapse epoch for the halo subunits. It is defined as the time when the linear rms density fluctuations at a scale corresponding to a fraction  $F$  of  $M_{\text{vir}}$  is equal to the linear collapse overdensity,  $\delta_c$ :

$$\sigma(FM_{\text{vir}}, a_c) = \delta_c(a_c). \quad (9)$$

Given the halo collapse epoch, the halo concentration is set via

$$c_{\text{vir}}(M_{\text{vir}}, a) = K_{\text{vir}} \frac{a}{a_c(M_{\text{vir}})}. \quad (10)$$

A closely related study by Wechsler et al. (2002, hereafter W02) showed that the B01 ‘‘collapse epoch’’ seems to correspond closely to the epoch when the mass accretion rate of the halo  $d \ln(M_{\text{vir}})/dt$ , is large compared to the rate of cosmic expansion. W02 found that if one defines the end of this rapid collapse phase to be when  $d \ln(M_{\text{vir}})/d \ln(a) \leq 2$ , it corresponds closely to the ‘‘formation epoch’’ in Eq. (9) above. After this epoch of rapid mass accretion ends, the halo mass and virial radius continue to grow via comparably minor mergers and diffuse mass accretion. These relatively minor mergers do not affect the inner regions of the halo ( $r < r_s$ ) significantly and so  $R_{\text{vir}}$  grows, but  $r_s$  remains approximately constant, leading to an increase in concentration as the halo evolves (W02).

The B01 model has two parameters,  $F$  and  $K$ , that have to be determined by calibrating them to numerical simulations. B01 analysed two  $\Lambda$ CDM simulations with  $\sigma_8 = 1.0$  and different resolutions and box sizes. Using a halo finder based on the Bound Density Maxima (BDM) algorithm (Klypin & Holtzman 1997), they assembled a catalogue of several thousand haloes for each simulation, and fit NFW profiles to each of them. B01 found that their model was able to satisfactorily reproduce the mean relation between halo mass and concentration, and the redshift dependence of the  $c_{\text{vir}}-M_{\text{vir}}$  relation with  $F = 0.01$  and  $K = 4.0$ . B01 and W02 determined that the scatter in concentration at fixed mass is well-described by a log-normal distribution with  $\sigma_{\log c} = 0.14$  dex. Other numerical studies have found a somewhat smaller scatter, with Jing (2000) reporting  $\sigma_{\log c} = 0.9 - 0.11$  dex, and Jing & Suto (2002) finding  $\sigma_{\log c} = 0.13$  dex.

The B01 model with  $F = 0.01$  and  $K = 4.0$  has since proven successful in reproducing concentrations of  $\Lambda$ CDM haloes over more than six orders of magnitude in halo mass from  $M_{\text{vir}} \simeq 10^7 M_\odot$  to  $M_{\text{vir}} \simeq 10^{13} M_\odot$  (e.g., Colín et al. 2003; Hayashi et al. 2003). However, as discussed in B01, the model ceases to make physical sense for halo masses large enough that  $FM_{\text{vir}}$  begins to approach the typical collapse mass at  $z = 0$ . This is because linear fluctuations stop growing at late times in  $\Lambda$ CDM, and with the simplified definition of collapse time discussed above, very large haloes never collapse. Consequently, the B01 model with  $F = 0.01$  underpredicts halo concentrations for systems more massive than a few  $\times 10^{14} M_\odot$  (e.g., Hayashi et al. 2003; Dolag et al. 2003). As a matter of pragmatism, this can be remedied with a simple change of parameters. With  $F = 0.001$  and  $K = 3.0$  the model works adequately for all masses, though it becomes somewhat less attractive because of the small value of  $F$ , for which the collapse epoch no longer corresponds directly to  $a_c$  defined by W02.

#### 3.2 The Analytic Model in Quintessence Cosmologies

As shown in § 2, linear overdensities have greater relative growth at higher redshift as  $w$  increases. We then expect, given an overdensity on a mass scale  $M_{\text{vir}}$ , that this mass

scale will collapse at higher redshift as we increase  $w$ . As the halo concentration reflects the density of the universe at the time of rapid collapse, we expect this change in average formation time to translate directly into a change in average concentration. The differences in  $w \neq -1$  models should be confined to changes in the rapid-collapse epoch  $a_c$  for haloes of a given mass.

From Equation (9),  $a_c$  for a halo of mass  $M_{\text{vir}}$  is determined by  $\delta_c$ ,  $D(a)$ , and  $\sigma_8$ . The changes in  $\delta_c$  with  $w$  (Figure 4) have a very small effect on  $a_c$ . More relevant are the changes in  $\sigma(M, a)$  and the linear growth rate (Fig. 3). For a fixed value of  $\sigma_8$  all the  $w$ -dependence of  $a_c(M_{\text{vir}})$  will be captured by  $D(a)$ , with  $\sigma(M, a)$  reaching the  $\delta_c$  collapse threshold at earlier times as  $w$  increases. We therefore expect concentrations to increase as  $w$  increases.

Note that an alternative definition of a halo's radius,  $R_{200}$ , the radius at which the mean halo density is equal to  $200\rho_{\text{crit}}$  has frequently been used in the past. This results in an alternative definition of concentration:  $c_{200} = R_{200}/r_s$  (e.g., NFW96). Of course, given a set of cosmological parameters, the model described above (and similar models) can be used to predict equivalent relations between  $c_{200}$  and  $M_{200}$ . For a fixed cosmology, the predicted relation between  $c_{200}$  and  $M_{200}$  will look quite similar to the  $c_{\text{vir}}-M_{\text{vir}}$  relation, with an offset that varies slowly as a function of concentration and accounts for the differences in values of the outer halo radius.

Because the simulations of B01 focused only on one cosmology, it was impossible to tell whether agreement with the simulations and the proposed B01 model was sensitive to the choice of defining halo concentration relative to  $R_{\text{vir}}$  instead of  $R_{200}$ . That is, one could have equally well proposed a different model based on  $c_{200}$ :

$$c_{200}(M_{200}, a) = \tilde{K}_{200} \frac{a}{a_c(M_{200})}. \quad (11)$$

The simulation results of B01 could have been reproduced using this model, simply by setting  $\tilde{K}_{200}$  equal to a slightly smaller value than the original  $K = 4.0$ .

Consider now the current case, where we compare simulation results based on cosmologies with different  $w$ 's and hence different  $\Delta_{\text{vir}}$  values. In these simulations, the ratios of  $R_{\text{vir}}/R_{200}$  (and  $c_{\text{vir}}/c_{200}$ ) for fixed-mass haloes will depend on the value  $\Delta_{\text{vir}}(w)$ . Therefore, it is impossible for a model based on  $c_{200}$  with fixed  $\tilde{K}_{200}$  to do equally well as the original B01 model based on  $c_{\text{vir}}$  with fixed  $K$  for all values of  $w$ . More physically, the original B01 model described above implicitly *assumes* that the haloes have virialized at the appropriate virial density and predicts that, in addition, the halo collapse redshift acts to set the ratio of the virial density ( $\propto R_{\text{vir}}^{-3}$ ) to the central density ( $\propto r_s^{-3}$ ). A model based on  $c_{200}$  with fixed  $\tilde{K}_{200}$  would instead assume that all of the changes in halo density arise solely because of changes in  $a_c$ . As we demonstrate below, the virial assumption seems to capture better our simulation results. It seems therefore, that there are two physical processes that set halo densities: one process is related to the global process of halo virialization and the other may be related to an earlier, rapid-collapse epoch.

## 4 NUMERICAL SIMULATIONS

In this section, we describe our numerical simulations. In § 4.1, we detail the numerical and cosmological parameters that were used. In § 4.3, we describe the methods we use to locate haloes and to fit NFW profiles to their density profiles.

### 4.1 Simulations and Parameters

We use GADGET version 1.1, a publicly-available and well-tested  $N$ -body code (Springel et al. 2001). Gravity between particles is solved using a hierarchical tree algorithm in co-moving coordinates, and both the force calculations and the time-stepping are performed in a fully adaptive way. Using the parallel version, we have run the code on either 96 375MHz IBM Power3 processors of NERSC's *Seaborg* or on 64 1.4GHz Athlon processors of *UpsAnd*, a 264-processor Beowulf cluster at The University of California at Santa Cruz. We made necessary alterations to the expansion rate of the universe for GADGET to account for quintessence cosmologies with  $w \neq -1$ .

Power et al. (2003) have performed a detailed convergence study of a high resolution cluster simulation using GADGET, and although we simulate a much larger cosmological volume we have followed their recommendations for a number of GADGET's parameters. In particular we have chosen an adaptive timestep equal to  $\Delta t_i = \eta_{a\epsilon} \sqrt{\epsilon_i/a_i}$ , where  $\epsilon_i$  and  $a_i$  are the gravitational softening and acceleration experienced by the  $i^{\text{th}}$  particle in the simulation, and  $\eta_{a\epsilon}$  is a dimensionless constant. Power et al. (2003) recommend setting  $\eta_{a\epsilon} = 0.2$ ; this choice of adaptive timestep minimizes undesirable effects due to particle discreteness and hard scatterings, while at the same time allowing for convergence at minimal computational expense. In GADGET, gravitational softening is performed using a cubic spline (Springel et al. 2001), for which the potential becomes exactly Newtonian at  $r = 2.8 \epsilon$ , where  $\epsilon$  is the softening length. Generally our simulations were run with a co-moving softening length of  $\epsilon = 2.5h^{-1}$  kpc, although we have run a few cases with  $\epsilon$  as low as  $1h^{-1}$  kpc.

Our cosmological background model is fixed by  $\Omega_M = 0.3$ ,  $\Omega_Q = 0.7$ ,  $h = 0.7$ , and  $n = 1.0$  for all values of  $w$ . In normalizing  $\sigma_8$  on the scale of galaxy clusters, the initial power spectra are nearly unaffected by quintessence. However, when normalizing to the scales probed by the CMB, the initial power spectra are altered by the inclusion of quintessence (section 2.2). As discussed below, we normalize our simulations such that  $\sigma_8 \simeq 0.74$ , thus the effect of  $w \neq -1$  is due almost exclusively to the expansion rate.

All of our simulations were run with  $256^3$  particles in boxes with sides of length  $60h^{-1}$  Mpc.  $\Omega_M = 0.3$  implies a mass per particle of  $M_p = 1.1 \times 10^9 h^{-1} M_\odot$ . For the analysis of halo concentrations we used only haloes with more than 100 particles (see §5.2). This corresponds to a minimum halo mass of  $M_{\text{vir}}^{\text{min}} \simeq 1.1 \times 10^{11} h^{-1} M_\odot$ , for which the B01 model predicts a median concentration of 13.5 (for  $\sigma_8 = 0.74$ ). This translates into an NFW scale radius of  $r_s^{\text{min}} \sim 10h^{-1}$  kpc. More massive haloes will have larger scale radii, and because even this minimum scale radius is almost three times larger than our softening length, we should be able to determine accurate concentrations from the haloes in our simulations.

**Table 1.** Simulation Parameters and Power Spectrum Normalizations.

Model $w$	$\epsilon/h^{-1}$ kpc	$\sigma_{8,\text{nom}}^a$	$\sigma_{8,\text{eff}}^a$
-0.50	2.5	0.742	0.799
-0.75	2.5	0.740	0.775
-1.00	2.5	0.738	0.716
-1.00	1.0	1.000	0.972
-1.25	2.5	0.736	0.716
-1.50	2.5	0.734	0.714

All other parameters are fixed at the same value for all simulations. The number of particles is  $N_p = 256^3$ , the box size is  $L_{\text{box}} = 60h^{-1}\text{Mpc}$ , and the initial redshift is  $z_i = 50$ . For all simulations, the remaining cosmological parameters are  $\Omega_M = 0.3$ ,  $\Omega_Q = 0.7$ ,  $h = 0.7$ , and  $n = 1.0$ .

<sup>a</sup> the difference between  $\sigma_{8,\text{nom}}$  and  $\sigma_{8,\text{eff}}$  is explained in §4.2.

Table 1 summarizes the parameters used in our simulations.

## 4.2 Initial Conditions

Setting initial conditions for our simulations requires fixing the  $z = 0$  power spectrum normalization, which we parameterize by  $\sigma_8$ . As discussed above (§2.2), our current understanding of present day clusters of galaxies makes  $\sigma_8$  still uncertain by  $\sim 20 - 30\%$  ( $\sigma_8 \sim 0.70 - 1.10$  for  $\Omega_M = 0.3$ ). Halo concentrations in cosmological N-body simulations depend sensitively on  $\sigma_8$ , because the amount of small-scale power directly affects typical halo formation times, especially for high mass haloes. For example, at  $M_{\text{vir}} = 10^{14} h^{-1} M_\odot$  the B01 model predicts median concentrations of  $c_{\text{vir}} = 6.8$  and  $c_{\text{vir}} = 5.3$  for  $\sigma_8 = 0.90$  and  $\sigma_8 = 0.74$ , respectively. We initialize our simulations with the values of  $\sigma_8$  determined by Kuhlen et al. (2004) from the abundance of clusters in the HIFLUGCS sample of local clusters (Reiprich & Böhringer 2002):  $\sigma_8 = 0.742, 0.740, 0.738, 0.736, 0.734$  for  $w = -1.50, -1.25, -1.00, -0.75, -0.50$ , respectively. We construct initial conditions for each  $w$  with the routines of the publicly-available PM code (Klypin & Holtzman 1997).

The process of initializing particle positions and velocities based on the linear power spectrum is subject to statistical fluctuations. The largest modes of the system ( $\lambda \simeq L_{\text{box}}$ ) are sampled only twice per dimension and are thus sensitive to deviations caused by small number statistics. As  $8h^{-1}$  Mpc is close to  $L_{\text{box}}$ , this can lead to noticeable differences between the “nominal” value of  $\sigma_{8,\text{nom}}$ , used to construct the initial conditions and an “effective” value of  $\sigma_{8,\text{eff}}$ , determined from the actual particle positions at the initial redshift. In order to quantify this difference, we determine  $\sigma_{8,\text{eff}}$  by direct numerical integration of the initial  $N$ -body power spectrum:

$$\sigma_{8,\text{eff}}^2 = \frac{1}{2\pi^2} \frac{D^2(z=0)}{D^2(z=50)} \int_0^\infty k^2 P_{\text{num}}(k) W(kR_8)^2 dk, \quad (12)$$

where  $P_{\text{num}}(k)$  is the power spectrum derived from the N-body initial conditions and  $W(x)$  is the spherical tophat window function given by  $W(x) = 3/x^2(\sin x/x - \cos x)$ , evaluated at  $kR_8$ , with  $R_8 = 8h^{-1}$  Mpc.

$P_{\text{num}}(k)$  only extends to  $k_{\text{min}} \approx 0.1h^{-1}\text{Mpc}^{-1}$ , which

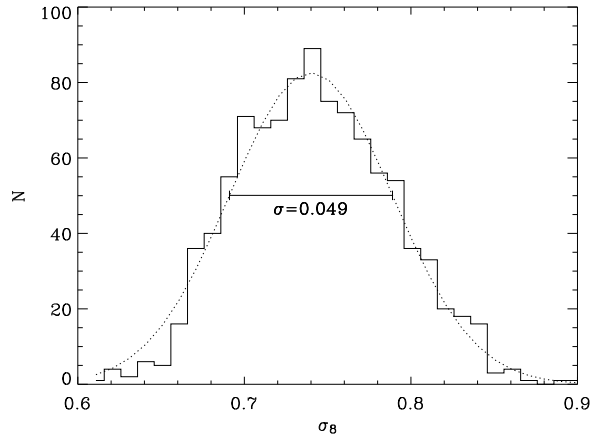


**Figure 5.** A histogram of the effective values of  $\sigma_8$  determined from 1000 Monte-Carlo realizations of the initial conditions with an input powerspectrum normalized to  $\sigma_8 = 0.74$ . The distribution is Gaussian with a standard deviation of 0.049, or roughly 7%.

is not low enough to allow the integral in Equation 12 to converge. We estimated the portion of the integral below  $k_{\text{min}}$  by integrating the smooth analytical power spectrum, and applied this correction to get  $\sigma_{8,\text{eff}}$ . We found that for  $w \leq -1$   $\sigma_{8,\text{eff}} \simeq 0.715$ , which is  $\sim 3\%$  lower than  $\sigma_{8,\text{nom}}$ . However, the variation of  $\sigma_8$  in a box of this size due to cosmic variance should be roughly  $\sim 5\%$ , so this difference is not surprising. To demonstrate this explicitly, we have constructed 1000 realizations of the initial conditions and computed values of  $\sigma_8$ . We infer from these realizations that measured values of the effective  $\sigma_8$  are distributed with a standard deviation of  $\sim 5\%$ . The resulting distribution is shown in Fig. 5. Therefore, the difference between  $\sigma_{8,\text{eff}}$  and  $\sigma_{8,\text{nom}}$  for the three  $w \leq -1$  cases is not surprising and is consistent with cosmic variance. We find similar deviations of  $\sigma_{8,\text{eff}}$  from  $\sigma_{8,\text{nom}}$  for all of the values of  $w$  that we simulate.

## 4.3 Halo Finders

We use two different halo finding algorithms to locate the haloes in our simulations, depending upon the quantities we probe with our simulation data. In § 5.1, we compare the mass functions of our simulated haloes with the J01 “universal” mass function. J01 used the Friends-Of-Friends (FoF) algorithm (Davis et al. 1985) to identify simulated haloes. In order to make a direct comparison to the J01 mass functions, we have employed a University of Washington FoF halo finder (<http://www-hpcc.astro.washington.edu/tools/fof.html>). As in J01 we set the linking length to 0.2 times the mean interparticle separation for all models.

To directly compare our halo concentrations to the B01 model (§ 5.2), we use an updated version of the halo finder that B01 and W02 employed in order to identify haloes. This halo finder is based on the BDM algorithm (Klypin & Holtzman 1997) and iteratively removes particles that are not bound to the halo in question. Upon identifying haloes, we fit NFW profiles to each halo and determine  $c_{\text{vir}}$ . For more



detail, we refer the reader to Appendix B of B01 and Appendix A of W02. We include in our catalogues only haloes with more than 100 particles, the same cut-off used by W02.

We have checked that both halo finding algorithms agree with each other, within our expectations, by comparing mass functions. The systematic differences in total mass between haloes defined in terms of the cosmology-dependent virial overdensity  $\Delta_{\text{vir}}(w)$  (as in the BDM finder) and those based on the fixed FoF linking length translate into only minor differences in mass functions. At high redshift, the two mass functions actually converge because  $\Delta_{\text{vir}}(z)$  approaches 178 and a linking length of 0.2 times the mean inter-particle separation roughly corresponds to a mean halo density of  $\sim 180 - 200$  times the background density. Below  $z \sim 2 - 2.5$ , the FoF and BDM mass functions agree well. At higher redshifts the BDM-based finder becomes increasingly incomplete. A consequence of the low value of  $\sigma_8$  in our simulations is that halo formation occurs more recently. Frequent merger events during the rapid mass growth phase of halo formation disrupt any spherical symmetry in the halo density profile. These haloes will not be well described by the NFW formula. In our implementation of the BDM halo finder, haloes with very bad fits to the NFW profile are rejected and not included in the catalogues. This is the major source of incompleteness at  $z \gtrsim 2.5$ . Note that the net effect of this incompleteness is to underestimate the number of low concentration haloes at high redshift.

## 5 RESULTS

### 5.1 Mass Functions

Several recent numerical studies have demonstrated that the J01 formula for halo mass functions may be considered “universal” as it accurately describes halo counts as a function of mass in  $N$ -body simulations of various cosmologies, including models containing dark energy with  $w \neq -1$  and a time-varying  $w$  (Linder & Jenkins 2003; Klypin et al. 2003; Macciò et al. 2003; Lokas, Bode, & Hoffman 2003). We confirm and further extend this conclusion by presenting halo mass functions from our simulations at different redshifts. In Figure 6, we show the mass functions of our FoF haloes in each cosmology and at a variety of redshifts from  $z = 0$  to  $z = 3$ . It is apparent that, in all panels, the mass functions and the redshift evolution of the mass functions for each  $w$  model are in excellent agreement with the J01 formula. Thus we confirm that the J01 formula is a good approximation at all redshifts for  $w > -1$  and we extend the range of validity of the J01 relation to include quintessence models with  $w < -1$ .

### 5.2 Concentrations

In §3.2, we described the manner in which quintessence modifies the predictions of the analytic B01 model for halo concentration as a function of mass. We have assembled catalogues consisting of more than  $\sim 1600$  haloes for each of our quintessence  $N$ -body simulations. The density profiles of every halo have been fit to an NFW profile, yielding a best-fit  $c_{\text{vir}}$  for each object. Some of these fits produced concentra-

tions smaller than one. We have excluded these haloes from our subsequent analysis.

The resulting  $c_{\text{vir}}(M_{\text{vir}})$  relations are plotted in Figure 7. We find that our simulations produce haloes with slightly lower concentrations than expected from previous simulation results (e.g., B01, Colín et al. 2003) and the analytic model proposed by B01 with  $F = 0.01$  and  $K = 4.0$ . However, we find that this difference can be described well by a constant offset. For example, keeping  $F = 0.01$  and lowering the proportionality constant  $K$  to  $K = 3.5$  [see Eq. 10] in the B01 model matches our data quite well for all of the  $w$  models we explore. We discuss this overall offset further in § 5.3. The  $c_{\text{vir}}-M_{\text{vir}}$  relation flattens out below  $M_{\text{vir}} \approx 6 \times 10^{11} h^{-1} M_{\odot}$ . We attribute this to the lower number of particles in these haloes, making them more susceptible to relaxation effects which tend to cause the central regions of haloes to be more diffuse and lead to lower concentrations. It is thus unlikely that this flattening represents any physical effect (compare to the results of Colín et al. 2003), and we have neglected the lowest mass bin in determining the best-fit value of  $K$ .

As mentioned above (§3.2), considering several cosmological models with different virial overdensities  $\Delta_{\text{vir}}$  allows us to distinguish between analytic prescriptions based on definitions of halo concentration in terms of  $R_{200}$ , in which the proportionality constant  $\tilde{K}_{200}$  is independent of cosmology (Eq. 11), and those based on the virial radius  $R_{\text{vir}}$ , in which  $K_{\text{vir}}$  is cosmology-independent (Eq. 10). To test this, we re-analysed the five  $z = 0$   $N$ -body outputs using the BDM halo finder, but setting  $\Delta_{\text{vir}} = \rho_{\text{vir}}/\rho_{\text{b}} = \rho_{\text{vir}}/\rho_{\text{crit}} \Omega_M^{-1} = 200 \Omega_M^{-1} \simeq 667$ , effectively yielding a relation between  $c_{200}$  and  $M_{200}$ . Matching these relations to the model described by Eq. 11 we determined best-fitting values of  $\tilde{K}_{200} = (3.76, 3.44, 3.32, 3.16, 3.16)$  for  $w = (-0.50, -0.75, -1.00, -1.25, -1.50)$ , respectively. This range in  $\tilde{K}_{200}$  is not consistent with one cosmology-independent value of  $\tilde{K}_{200}$ . The results of this analysis suggest that models similar to the B01 model, in which the halo concentration is defined in terms of  $R_{\text{vir}}$  and  $\Delta_{\text{vir}}$ , are more readily generalizable to alternative cosmologies as  $c_{\text{vir}}$  is related to  $a/a_c$  via a *cosmology-independent* constant of proportionality,  $K_{\text{vir}}$ . Put another way, defining the radius of a halo, and thus its concentration, using a fixed overdensity criterion necessitates using a cosmology-dependent proportionality constant in Eq. (10) while the cosmology-dependent virial overdensity definition seems to account for these differences, so that  $K_{\text{vir}}$  is independent of cosmology.

As in previous studies (B01; Jing 2000; Jing & Suto 2002), we also find that haloes of a given mass have a broad distribution of concentrations. To determine the inherent scatter in the  $c_{\text{vir}}-M_{\text{vir}}$  relation it is important to account for the artificial scatter introduced by uncertainties in the fit to an NFW profile and by the Poisson noise in each bin. Following the B01 analysis, we corrected for the former by determining 500 one-sided Gaussian deviates for each halo with a standard deviation equal to the error in the  $c_{\text{vir}}$  fit returned by the halo finder. The deviates are positive (negative) if  $c_{\text{vir}}$  is less (greater) than the median in that bin. We then determined the 16<sup>th</sup> and 84<sup>th</sup> percentiles in  $\log(c_{\text{vir}})$  and subtract off the Poisson noise from each in quadrature. The resulting estimates of the intrinsic scatter are shown as the dashed lines in Figure 7. The scatter is consistent with

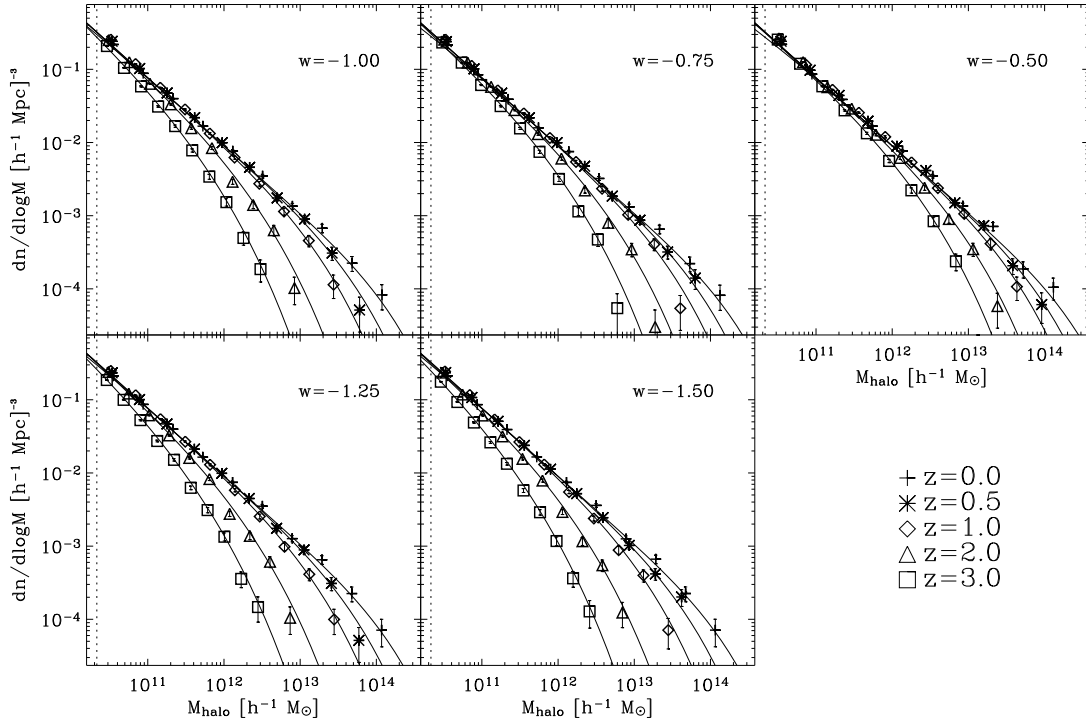


**Figure 6.** A comparison between the J01 analytic mass function (solid lines) and the mass functions derived from our five N-body simulations (shapes with error bars, see the legend in the lower right portion of the Figure). The haloes in our simulations were located using a FoF algorithm with a linking length equal to 0.2 times the mean particle separation as in J01. In each panel we plot mass functions at various redshifts, from top to bottom:  $z = 0.0, 0.5, 1.0, 2.0,$  and  $3.0$ . The error bars represent the Poisson noise due to the finite number of haloes in each mass bin.

being independent of  $w$  and  $M_{\text{vir}}$ , and we find that taking the B01 proportionality constant to be  $K_{\text{low}} = 2.28$  and  $K_{\text{high}} = 4.52$  fits the lower and upper lines well. These values correspond to  $\sigma_{\log c, \text{low}} = 0.18$  dex and  $\sigma_{\log c, \text{high}} = 0.11$  dex. Although these are similar in magnitude to the scatter reported in previous studies, our distributions are skewed away from log-normal toward lower concentrations. We note that the skewness may likely be caused by the lower resolution of our simulations, which tends to result in lower concentration haloes.

For a fixed mass the B01 model predicts that concentration should decrease with redshift as  $1/(1+z)$ . The haloes in our simulation also satisfy this relation, as shown by Figure 8, in which we plot the redshift dependence of concentration for haloes of mass  $M_{\text{vir}} = 7 \times 10^{11} h^{-1} M_{\odot}$ . This figure shows that the concentrations follow the  $c_{\text{vir}} \propto (1+z)^{-1}$  relation that is embodied in the B01 analytic model. At redshifts greater than  $\sim 2.5$ , our catalogues of haloes in this mass bin with fitted NFW profiles become incomplete. This incompleteness preferentially affects low concentration haloes, causing the  $c_{\text{vir}}(z)$  relation to flatten at high redshift. We do not believe this to be a physical effect, and trust our data points to  $z \sim 2.5$ .

### 5.3 The Concentration Discrepancy

We have attempted to understand the origin of the discrepancy between  $c_{\text{vir}}(M_{\text{vir}})$  derived from our simulations and those reported by B01 and summarized by the B01 model. We have re-analysed the same  $z = 0$  simulation data that was analysed previously by B01, and we were able to reproduce their  $c_{\text{vir}}-M_{\text{vir}}$  relation and scatter. We conclude that the discrepancy that we observe is not due to any change in analysis procedures.

Of course, the main difference between the study of B01 and our work is the choice of simulation codes. Whereas we use the publicly-available, uniform-resolution code GADGET, B01 used the adaptive-refinement code ART. Undoubtedly the effective resolution at the centres of haloes was higher in the B01 simulation than in ours. In order to shed further light on this matter, we have run one additional GADGET simulation designed to test the importance of the effective force resolution. Compared to the five simulations discussed previously, this one has higher force resolution ( $\epsilon = 1.0 h^{-1}$  kpc) and  $\sigma_8 = 1.0$ . The resulting  $c_{\text{vir}}(M_{\text{vir}})$  relation is shown in Figure 9.

Here, we again find that the GADGET concentrations are systematically lower than the ones found by B01 with ART by  $\sim 14\%$ . Instead of  $K = 4.0$  we find  $K = 3.44$  matches the GADGET halo concentrations. This is consistent with the value found for the five lower resolution

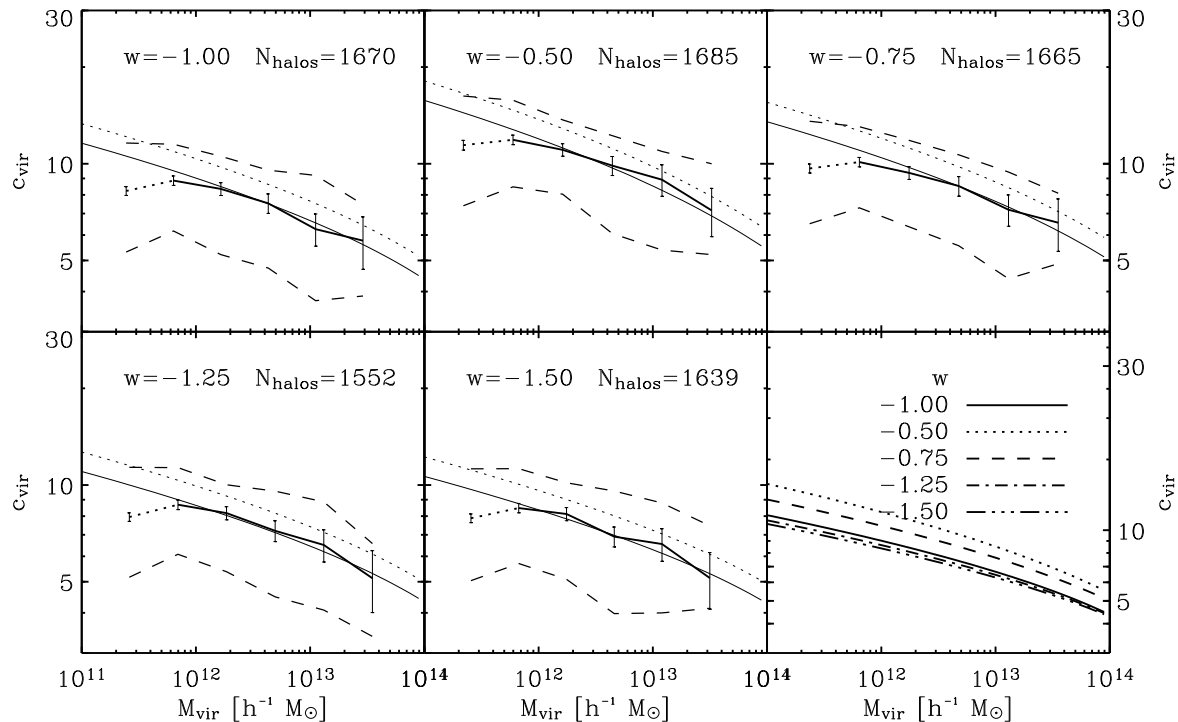


**Figure 7.** The concentration parameter  $c_{\text{vir}}$ , as a function of mass  $M_{\text{vir}}$ , for the five quintessence N-body simulations. The original ( $F = 0.01, K = 4.0$ ) and our best-fitting ( $F = 0.01, K = 3.5$ ) B01 models are over-plotted as thin dotted and solid lines, respectively. Error bars represent the Poisson noise due to the finite number of haloes per bin. The dashed lines are our estimates of the intrinsic scatter in the relation, obtained by removing the scatter due to errors in the fits of the NFW profiles, as well as Poisson noise. The lowest mass bin was excluded in our analysis and is shown here for completeness only. The total number of haloes in the remaining bins is shown in the upper right corner of each panel. The lower right panel shows the best-fitting B01 model for all five values of  $w$ .

quintessence simulations described above. The difference in  $K$  between our simulations and the B01 simulation may be due to an inherent difference between the GADGET and ART N-body codes. Whether this is due to the higher maximum force resolution afforded by the adaptive refinement of ART, or another difference between the two codes remains unclear.

Several recent analyses based on  $w = -1$  simulations with higher resolution than our own (Hayashi et al. 2003; Colín et al. 2003; Tasitsiomi et al. 2003) also favor the B01 model with  $K = 4.0$ . In light of these results we suggest that our GADGET simulations systematically under-predict halo concentrations by  $\sim 10 - 15\%$ . However, when this offset is normalized out, the variation of  $c_{\text{vir}}(M_{\text{vir}})$  with  $w$  scales as predicted, and we conclude that the B01 model is successful in this regard. Emboldened by this success, we use the model to explore the implications of various normalization choices and to compare expected halo densities with those inferred from galaxy rotation curves. In what follows, we assume  $K = 4.0$  for the model normalization and we advocate this choice for the reasons outlined above. (However, setting  $K = 3.5$  would not qualitatively change the conclusions that follow.)

## 6 HALO CONCENTRATIONS AND CENTRAL DENSITIES WITH $w \neq -1$

In Figure 10, we illustrate the degeneracy between  $w$  and  $\sigma_8$  in setting halo concentrations. Shown are the predictions of the B01 model ( $F = 0.01, K = 4.0$ ) for  $c_{\text{vir}}(z = 0)$  with a fixed normalization  $\sigma_8 = 0.74$  for several values of  $w$ . As discussed in § 3.2, for a fixed normalization, concentrations increase as  $w$  increases because haloes collapse earlier. The right panel of the figure shows the corresponding predictions for  $c_{\text{vir}}$  with  $\sigma_8$  determined by normalizing to the CMB with  $\tau = 0$  (see § 2.3). Note that for the CMB normalization, the trend with  $w$  is in the opposite direction, with increasing  $w$  implying lower concentrations. As illustrated in Figure 2, higher  $w$  requires a lower normalization:  $\sigma_8 \simeq 0.6, 0.9,$  and  $1.0$  for  $w = -0.5, -1,$  and  $-1.5$ , respectively. The change in normalization based on the CMB dominates changes in the growth function that give rise to the behavior of  $c_{\text{vir}}(w)$  at fixed normalization.

As discussed previously, the  $c_{\text{vir}}$  parameter is useful, but it is not a direct measure of physical density. We would like, therefore to convert our predicted  $c_{\text{vir}}$  relations into quantities that have a more direct physical interpretation, and are more amenable to comparison with observations. Alam, Bullock, & Weinberg (2002) proposed the *central density parameter* as a means to quantify the physical density in the central regions of a galaxy:

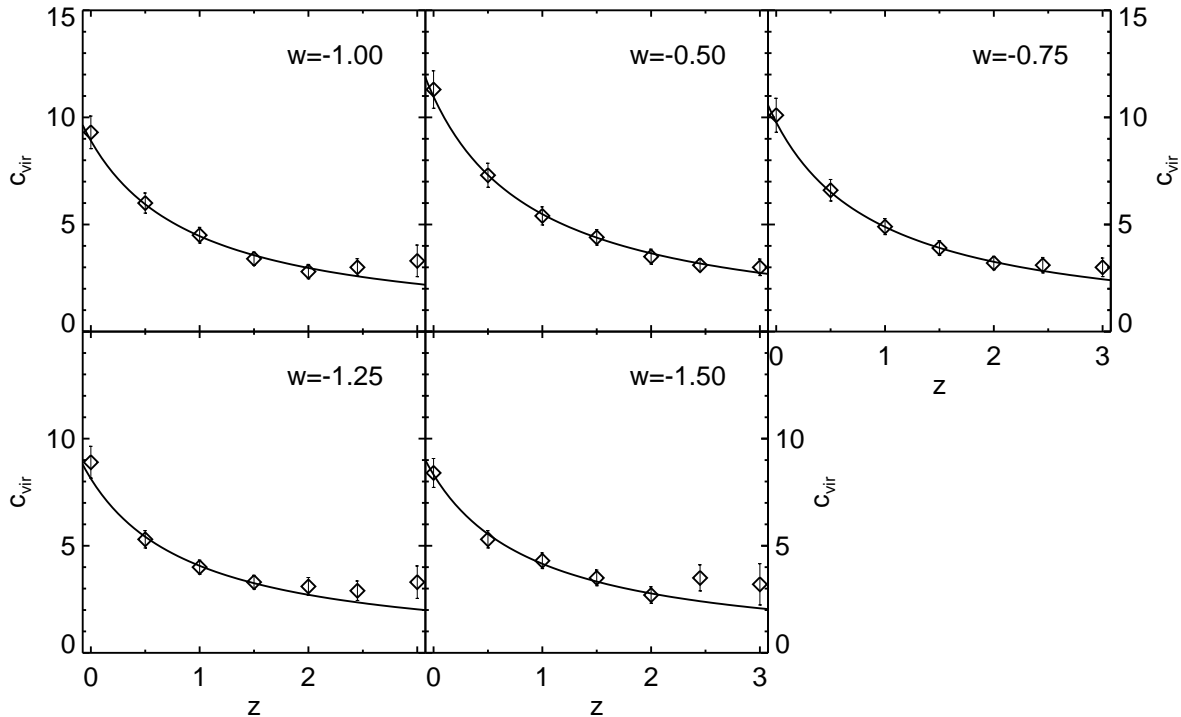


**Figure 8.** The median concentrations of haloes in bins of mass  $M_{\text{vir}} = 7 \times 10^{11} h^{-1} M_{\odot} \pm 0.05$  dex as a function of redshift. Error bars represent the Poisson noise due to the finite number of haloes per bin.  $c_{\text{vir}}$  falls in proportion to  $1/(1+z)$  (solid lines), in agreement with the B01 model. The flattening at  $z \gtrsim 2.5$  is probably not physical, and may be caused by incompleteness in the halo catalogues at high redshift which preferentially excludes low concentration haloes.

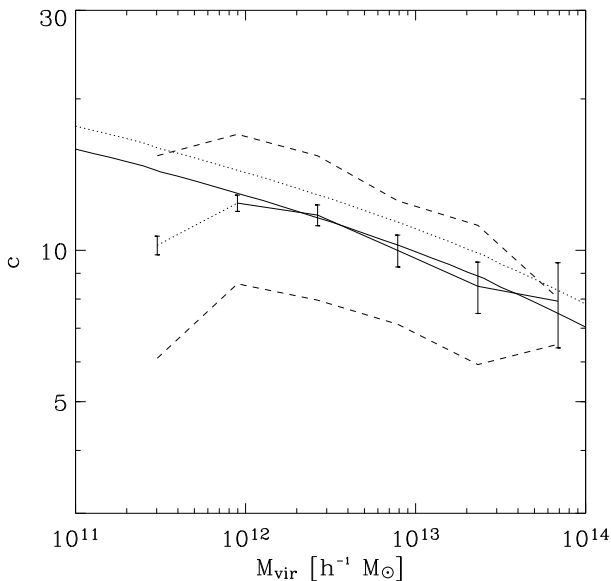


**Figure 9.**  $c_{\text{vir}}(M_{\text{vir}})$  for our high resolution ( $\epsilon = 1.0 h^{-1}$  kpc)  $\sigma_8 = 1.0$  GADGET simulation designed to approximate the adaptive-refinement ART simulation used in B01. The original B01 relation is overplotted as a dotted line. The dotted line segment and the dashed lines are as in Fig. 7.

$$\Delta_{V/2} \equiv \frac{1}{2} \left( \frac{V_{\text{max}}}{H_0 r_{V/2}} \right)^2. \quad (13)$$

$\Delta_{V/2}$  is the mean overdensity within  $r_{V/2}$ , the radius at which the galaxy rotation curve reaches half its maximum,  $V_{\text{max}}$ .

The  $\Delta_{V/2}$  parameter is advantageous for several reasons. First, it facilitates comparisons between theory and observation. Any predicted  $c_{\text{vir}}$  vs.  $M_{\text{vir}}$  relation can be easily converted into a  $\Delta_{V/2}$  vs.  $V_{\text{max}}$  relation. Similarly, given an observed galaxy rotation curve,  $\Delta_{V/2}$  can be determined without reference to any particular analytic density profile. It also has the useful characteristic that even if an observed rotation curve is rising at the last measured point, substituting the highest (outer) most point on the rotation curve for  $V_{\text{max}}$  in the formula above results in an *upper limit* on the true value of  $\Delta_{V/2}$ . Specifically, if  $V_{\text{max}}$  is underestimated by a factor  $f_v$ , and the density profile varies with radius as  $\rho(r) \propto r^{-\alpha}$ , this leads to an overestimate of  $\Delta_{V/2}$  by a factor of  $f_v^{-2\alpha/(2-\alpha)}$ . Thus this is an overestimate so long as the density profile falls off with radius or is constant. Furthermore, if  $\alpha > 2/3$ , the fractional overestimate of  $\Delta_{V/2}$  is larger than the fractional underestimate of  $V_{\text{max}}$ .

We compare the B01 model predictions in terms of these quantities in Figure 11 for three representative quintessence cosmologies to the observational data of low-surface brightness and dwarf galaxies compiled by Zentner & Bullock (2002; the same set of observed galaxies are discussed in

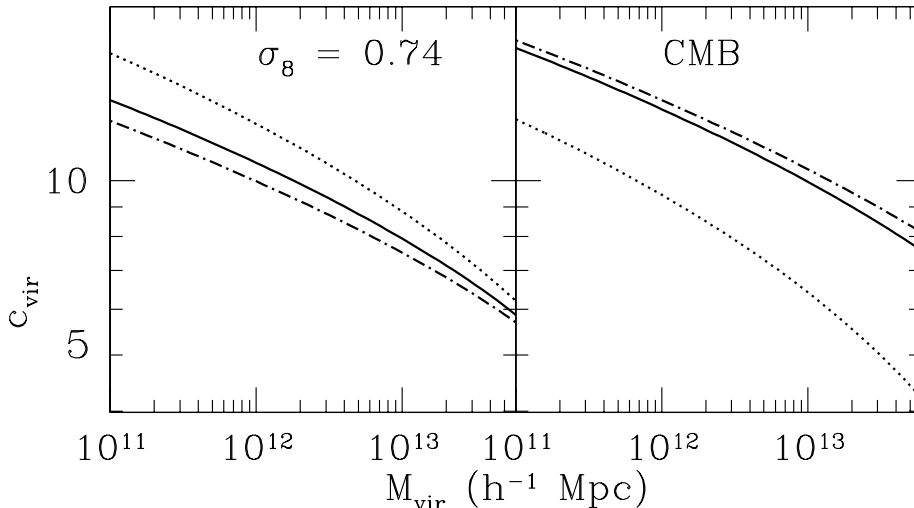


**Figure 10.** Predictions for halo concentration as a function of  $M_{\text{vir}}$ . Dotted, solid, and dash-dot lines in each panel refer to  $w = -0.5, -1$ , and  $-1.5$ , respectively. The left panel is for the fixed  $\sigma_8$  used in the simulations presented in this paper. The right panel shows how the halo concentration changes when we normalize based on the CMB:  $\sigma_8 \simeq 0.6, 0.9$ , and  $1.0$  for  $w = -0.5, -1$ , and  $-1.5$ , respectively.

Hayashi et al. 2003, who reach similar conclusions) from the observational work of Swaters (1999), de Blok, McGaugh, & Rubin (2001), and de Blok and Bosma (2002). The error bar in the right panel shows the theoretical  $1\sigma$  scatter in  $\Delta_{V/2}$  expected at fixed  $V_{\text{max}}$  due to the scatter in  $c_{\text{vir}}$ .

While it is difficult to quantify the agreement of each quintessence cosmology with observational data, the cosmological model that is most commonly referred to as the standard, concordance cosmological model with  $w = -1$  ( $\sigma_8 = 0.9$ , solid line, right panel) seems to be in conflict with the extant observational data. For  $w = -1$ , lowering the normalization of the power spectrum to the value  $\sigma_8 \approx 0.74$  (solid line, left panel) can greatly alleviate this discrepancy (Alam, Bullock, & Weinberg 2002; Zentner & Bullock 2002; McGaugh et al. 2003). However, a  $w = -0.5$  model with the same  $\sigma_8 \approx 0.74$  normalization (dotted line, left panel) does not do as well because earlier structure formation produces higher galactic central densities.

Notice that the trends with  $\Delta_{V/2}$  for fixed  $V_{\text{max}}$  do not scale as might be expected from the  $c_{\text{vir}}$  trends at fixed mass shown in Figure 10. This is because  $\Delta_{V/2}$  is a physical measure of density and it increases not only with  $c_{\text{vir}}$  but also with  $\Delta_{\text{vir}}$  (i.e. haloes are defined with respect to different overdensities). This effect is most apparent when comparing the right panels of Figures 10 and 11. Though the concentrations of haloes with  $w = -0.5$  and  $\sigma_8 = 0.6$  (dotted-line, right panel, Figure 10) are much lower than those in the standard  $w = -1.0$ ,  $\sigma_8 = 0.9$  case (solid line, right panel), the actual densities of those haloes are roughly the same in the right panel of Figure 11. This is because  $w = -0.5$  models have higher virial densities (see Figure 4). Even though haloes in the low-normalization  $w = -0.5$  model tend to have the same (rapid-collapse) formation epoch as those in the higher-normalization  $w = -1$  model, the higher virial densities in the former model make the haloes denser overall.

By inspecting Figure 11, we can immediately determine that models with  $w < -1$  and moderately low  $\sigma_8$  ( $\sigma_8 \sim 0.7 -$

0.8) can bring theoretical predictions to rough agreement with rotation curve data from low surface brightness and dwarf galaxies. Though it is clear that sufficiently decreasing  $\sigma_8$  can bring any model into accord with the median of the data, a  $w = -0.5$  model would require  $\sigma_8 < 0.6$ . Such a low normalization would be nearly impossible to reconcile with  $z = 0$  cluster abundance data. Thus from the standpoint of quintessence, models with  $w < -1$  seem mildly favored by galaxy density data. Conversely, models with  $w$  as high as  $\sim -0.5$  are strongly disfavored by galactic rotation curves coupled with only a weak prior on the normalization of the power spectrum.

Note that none of the models can easily account for the very low data points. Nevertheless, the scatter in the data is not extremely large compared to the scatter expected from the halo-to-halo variations observed in N-body simulations. For example, at  $V_{\text{max}} = 80$  km/s, the  $1\sigma$  scatter in N-body simulations is  $\sigma(\log(\Delta_{V/2})) \simeq 0.37$  while the  $1\sigma$  scatter in all 67 data points is  $\sigma(\log(\Delta_{V/2})) \simeq 0.41$ . This suggests that lowering the median of the theoretically predicted central densities, perhaps by a reduction in  $\sigma_8$  or invoking a tilted or running power spectrum that reduces power on galaxy scales, or as we discuss here, by invoking  $w < -1$  quintessence, may be sufficient to bring the predictions into good agreement with the data. Yet, we must bear in mind that our calculations are approximate. The most obvious omission is that all of our calculations are based on N-body simulations that contain no baryons. The effects of baryonic contraction are likely to be small in LSB galaxies (e.g., de Blok & McGaugh 1997) and would tend to drive rotation curves to higher values of  $\Delta_{V/2}$  and  $V_{\text{max}}$  in the simplest models (Blumenthal et al. 1986). This serves only to increase the apparent discrepancy. Additionally, rotation curve measurements may yet be subject to poorly-understood systematic effects in the reduction of the observational data (Swaters et al. 2003). Currently, it is difficult to draw a firm conclusion.

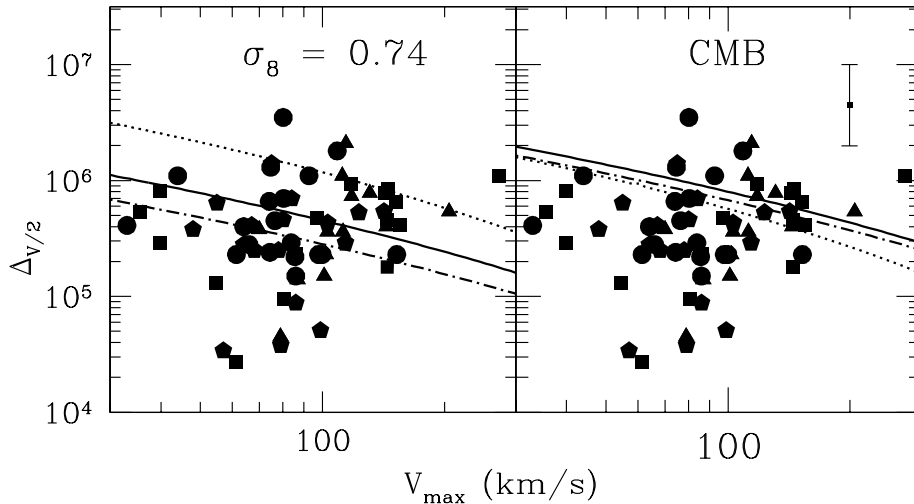


**Figure 11.** The central density parameter as a function of the maximum halo circular velocity. Dotted, solid, and dash-dot lines in each panel refer to  $w = -0.5, -1$ , and  $-1.5$ , respectively. The left panel is for a fixed  $\sigma_8 = 0.74$  and the right panel is normalized to match the CMB:  $\sigma_8 \simeq 0.6, 0.9$ , and  $1.0$  for  $w = -0.5, -1$ , and  $-1.5$ , respectively. The error bar in the right panel shows the expected theoretical  $1 - \sigma$  scatter in  $\Delta_{V/2}$  due to the scatter in  $c_{\text{vir}}$ . The points are for observed LSB and dwarf galaxies (see text for references).

## 7 SUMMARY AND CONCLUSIONS

Although the nature of dark energy is unknown, its effects on structure formation can be studied using numerical N-body simulations. We have performed a series of these simulations for a range of dark energy equation of state parameters. Confirming previous findings by Linder & Jenkins (2003), Klypin et al. (2003), Macciò et al. (2003), and Lokas et al. (2003) we show that the J01 formula provides a good fit to halo mass functions even in the presence of non- $\Lambda$ CDM dark energy. We show that this is true for models with  $w < -1$  as well.

The density structure of dark matter haloes is also affected by dark energy. We have shown how the predictions of the B01 model are modified when dark energy with constant  $w$  is accounted for. As structure tends to form earlier in models with less negative  $w$ , halo concentrations tend to be somewhat higher in these models. These findings are in agreement with the results of Klypin et al. (2003) and qualitatively agree with Dolag et al. (2003), although we probe a different range of masses than the latter. The larger number of haloes with NFW profile fits and concentrations in our study allows us to quantitatively test the B01 model. We find that the original ( $F = 0.01, K = 4.0$ ) over-predicts the concentrations of haloes in our simulations by about  $\sim 12\text{--}15\%$ . However, the shape of the mass-concentration relation that we find is the same as in B01, and we find that a slightly modified set of the B01 parameters ( $F = 0.01, K = 3.5$ ) matches our haloes well. This offset may likely be caused by the lower force resolution of our GADGET simulations compared to the adaptive-refinement code ART used in B01. For the haloes in our simulations the adopted B01 model accurately reproduces the median concentration-mass relation over a range of masses from  $M_{\text{vir}} \sim 6 \times 10^{11}$  to  $M_{\text{vir}} \sim 4 \times 10^{13} h^{-1} M_{\odot}$ . We confirm that for a fixed mass halo concentration decrease with redshift as  $1/(1+z)$ , at least out to  $z \sim 2.5$ .

Interestingly, we find that halo concentrations are more

easily understood when the halo virial radius is defined in terms of a cosmology-dependent virial overdensity rather than by one that uses a fixed overdensity of  $\rho/\rho_{\text{crit}} = 200$ . The result supports one of the (previously-untested) assumptions of the original B01 model. Specifically, we argue that halo densities in different cosmological models are influenced both by changes in the overall virialization process of haloes as well as by changes in epoch when the halo cores collapse. As noted in §6, it is important to include both of these physical processes when comparing predictions for galaxy densities to real data, as in Figure 11.

Having confirmed that the B01 model correctly describes the scaling of halo concentrations as a function of mass and redshift even in cosmologies with  $w \neq -1$ , we have investigated the effects of dark energy on a comparison between model predictions and observations of central halo densities. Zentner and Bullock (2002) found that the observed distribution of  $\Delta_{V/2}$  as a function of  $V_{\text{max}}$  is inconsistent with the predictions of the B01 model for  $\Lambda$ CDM and  $\sigma_8 = 0.9$ . The model predicts haloes that are simply too concentrated (see also Primack 2003). A lower value of  $\sigma_8 = 0.75$ , as used in our simulations, can alleviate this discrepancy, but such models may face other difficulties regarding early reionization (Somerville, Bullock, & Livio 2003) and possibly with reproducing the properties of halo substructure (Zentner & Bullock 2003). Including the effects of dark energy, we find that for models with  $w > -1$  the problem is exacerbated because haloes collapse earlier and because they have higher virial overdensities. Note that for the extreme case of  $w = -0.5$ , even a normalization as low as  $\sigma_8 = 0.6$  seems disfavored by the data. Thus one interesting conclusion is that the rotation curves of galaxies coupled only with a weak prior on the normalization of the power spectrum of density fluctuations seem to disfavor quintessence models with  $w$  significantly larger than  $-1$  without measuring the expansion history of the Universe, as is done in SNIa analyses. Models with  $w < -1$  do better,

and can tolerate higher values of  $\sigma_8 \sim 0.8$ , but not high as high as  $\sigma_8 \sim 1$ , as is suggested the CMB normalization.<sup>2</sup>

As we have pointed out throughout this paper, there have been a number of previous studies of the effects of dark energy ( $w \neq -1$ ) on dark matter halo abundances and concentrations. Here we summarize how this work distinguishes itself from these past efforts. We have shown for the first time how results for  $\Delta_{\text{vir}}$  and the linear transfer function are modified for dark energy with  $w < -1$ . In addition we have expanded on previous studies (Schuecker et al. 2003) of  $\delta_c$  in phantom cosmologies. We have pointed out that there are significant differences in the amplitude and  $w$ -dependence of  $\sigma_8$  between normalizations based on the CMB and galaxy cluster abundances. For the first time we have been able to draw a distinction between a definition of concentration based on a cosmology-dependent  $R_{\text{vir}}$  and constant  $R_{200}$ , and found that our simulations prefer the former. Unlike previous studies of the effects of dark energy on halo concentrations (Klypin et al. 2003; Dolag et al. 2003), which analysed a small number of pre-selected haloes, we have performed an analysis of  $\sim 1600$  haloes in each simulation. This allowed us to directly test the B01 model for  $c(M, z)$  with statistical significance. Furthermore these previous studies focused on group- and cluster-sized haloes, whereas we have extended this study down to galaxy mass haloes. Lastly, we have shown for the first time how different values of  $w$  and power spectrum normalizations affect the theoretical predictions of  $\Delta_{V/2}$  vs.  $V_{\text{max}}$ . A comparison to observations shows that models with  $w$  as low as  $-0.50$  are strongly disfavored for any value of  $\sigma_8$ , standard  $\Lambda$ CDM models require  $\sigma_8 \lesssim 0.8$ , and models with  $w < -1$  can accomodate higher values of  $\sigma_8$ .

As future observations further constrain the nature of dark energy, it will become necessary to extend these types of studies to more realistic models of dark energy. Future simulations with higher mass and force resolution, including the effects of baryons, and incorporating more realistic dark energy models will further advance our understanding of the interplay between cosmology and dark matter halo structure.

We thank P. Madau for interesting and helpful discussions. MK is supported by NSF grant AST-0205738. LES is supported by the Department of Energy grant DE-FG02-91ER40690. ARZ is supported by The Center for Cosmological Physics at The University of Chicago under NSF PHY 0114422. JSB is supported by NASA through Hubble Fellowship grant HF-01146.01-A from the Space Telescope Science Institute, which is operated by the Association of Universities for Research in Astronomy, Incorporated, under NASA contract NAS5-26555. JRP is supported by NSF grant AST-0205944. ARZ thanks The Center for Cosmology and Particle Physics at New York University for their hospitality during several visits while this work was in progress. We thank V. Springel for use of the publicly-available code GADGET and we than U. Seljak and M. Zaldarriaga for use of the publicly-available code CMBFAST.

## REFERENCES

- Alam S. M. K., Bullock J. S., Weinberg D. H., 2002, ApJ, 572, 34  
 Allen P. R., Trilling D. E., Koerner D. W., Reid I. N., 2003, ApJ, 595, 1206  
 Barris J. B., et al. , 2003, ApJ, 602, 571  
 Bartelmann M., Perotta F., Baccigalupi C., 2002, A&A, 396, 21  
 Blumenthal G. R., Faber S. M., Flores R., Primack J. R., 1986, ApJ, 301, 27  
 Bucher M., Spergel D., 1999, Phys. Rev. D, 60, 043505  
 Bullock J. S., et al. , 2001, MNRAS, 321, 559 (B01)  
 Bullock J. S. 2002, The shapes of galaxies and their dark haloes, Proceedings of the Yale Cosmology Workshop "The Shapes of Galaxies and Their Dark Matter Halos", New Haven, Connecticut, USA, 28-30 May 2001. Edited by Priyamvada Natarajan. Singapore: World Scientific, 2002, ISBN 9810248482, p.109, 109  
 Caldwell R. R., 2002, Phys. Lett. B, 545, 23  
 Caldwell R. R., Dave R., Steinhardt P. J., 1998, Phys. Rev. Letters, 80, 1582  
 Carlstrom J. E., Holder G., and Reese E. D., 2001, ARAA, 40, 643  
 Carroll S. M., Hoffman M., Trodden M., 2003, Phys. Rev. D, 68, 023509  
 Cline, J. M., Jeon S., & Moore, G. D., 2003, Phys. Rev. D, submitted, (preprint: hep-ph/0311312)  
 Colín P., Klypin A. A., Valenzuela O., Gottlöber S., 2003, ApJ, submitted, (preprint: astro-ph/0308348)  
 Dave R., Caldwell R. R., Steinhardt P. J., 2002, Phys. Rev. D, 66, 023516  
 Davis M., Efstathiou G., Frenk C. S., White S. D. M., 1985, ApJ, 292, 371  
 de Blok W. J. G., McGaugh S. S., 1997, MNRAS, 290, 533  
 de Blok W. J. G., McGaugh S. S., Rubin V. C., 2001, AJ, 122, 2396  
 de Blok W. J. G., Bosma A. A., McGaugh S. S., 2003, MNRAS 340, 657  
 Dodelson S., et al. , 2002, ApJ, 572, 140  
 Dolag K., Bartelmann, M., Perrotta, F., Baccigalupi, C., Moscardini, L., Meneghetti, M., Tormen, G., 2003, A&A, 416, 853  
 Eke V. R., Navarro J. F., Steinmetz M., 2001, ApJ, 554, 114  
 Flores R., Bullock J. S., Kravtsov A. V., Allgood B., Primack J. R., 2004, in preparation  
 Ghigna S., Moore B., Governato F., Lake G., Quinn T., Stadel J., 1998, MNRAS, 300, 146  
 Hayashi E., et al. , 2003, MNRAS, submitted (preprint: astro-ph/0310576)  
 Hoekstra H., Yee H. K. C., Gladders M. D., 2003, ApJ, in print (preprint: astro-ph/0306515)  
 Hu W., Sugiyama N., 1995, ApJ, 444, 489  
 Hu. W., Jain B., 2003, Phys. Rev. D, submitted (pre-print: astro-ph/0312395)  
 Huterer D., Ma C.-P., 2004, ApJ, 600, L7  
 Jenkins A., et al. , 2001, MNRAS, 321, 372 (J01)  
 Jing Y. P., 2000, ApJ, 535, 30  
 Jing Y. P., Suto S., 2002, ApJ, 574, 538  
 Klypin A. A., Holtzman J., 1997, astro-ph/9712217  
 Klypin A. A., Kravtsov A. V., Bullock J. S., Primack J. R., 2001, ApJ, 554, 903  
 Klypin A. A., Macciò A. V., Mainini R., Bonometto S. A., 2003, ApJ, 599, 31  
 Knop R.A. et al. , 2003, ApJ, 598, 102  
 Kravtsov A. V., Klypin A. A., Khokhlov A. M., 1997, ApJS, 111, 73  
 Kuhlen M., Keeton C. R., Madau P., 2004, ApJ, 601, 104  
 Kujat J., Linn A. M., Scherrer R. J., Weinberg D. H., 2002, ApJ, 572, 1  
 Lacey C., Cole S., 1993, MNRAS, 262, 627

<sup>2</sup> Note that using  $K = 3.5$  instead of  $K = 4.0$  would not change any of the conclusions regarding galaxy rotation curves and the central density problem.

- Lee J., Shandarin S.F., 1999, ApJ, 517, L5
- Linder E. V., Jenkins A., 2003, MNRAS, 346, 573
- Lokas E. L., Bode P., Hoffman Y., 2004, MNRAS, 349, 595
- Ma C.-P., Bertschinger E., 1995 ApJ, 455, 7
- Ma C.-P., Caldwell R. R. Bode, P. Wang L., 1999 ApJ, 521, L1
- Macciò A. V., Quercellini C., Mainini R., Amendola L., Bonometto S. A., 2003, Phys. Rev. D, submitted (preprint: astro-ph/0309671)
- Mainini, R., Macciò A. V., & Bonometto, S. A., 2003, New Astronomy, 8, 173
- Molinari E., Zacchei A., 2002, ApJ, 575, 801
- McGaugh S. S., Barker M., de Blok W. J. G., 2003, ApJ, 584, 566
- Monaco P., 1995, ApJ, 447, 23
- Mota, D. F., & van de Bruck, C., 2004, A&A, 421, 71
- Navarro J. F., Frenk C. S., White S. D. M., 1995, MNRAS, 275, 56
- Navarro J. F., Frenk C. S., White S. D. M., 1996, ApJ, 462, 563
- Navarro J. F., Frenk C. S., White S. D. M., 1997, ApJ, 490, 493
- Navarro J. F., et al. , 2003, MNRAS, in print (preprint: astro-ph/0311231)
- Perlmutter S., et al. , 1999, ApJ, 517, 565
- Pierpaoli E., Scott D., White M., 2001, MNRAS, 325, 77
- Pierpaoli E., Borgani S., Scott D., White M., 2003, MNRAS, 342, 163
- Power C., Navarro J. F., Jenkins A., Frenk C. S., White S. D. M., Springel V., Stadel J., Quinn T., 2003, MNRAS, 338, 14
- Press W. H., Schechter P., 1974, ApJ, 187, 425
- Primack J. R., 2003, IAU 220 Proceedings (pre-print: astro-ph/0312459)
- Ratra B., Peebles P. J. E., 1988, Phys. Rev. D, 37, 3406
- Reiprich T. H., Böhringer H., 2002, ApJ, 567, 716
- Riess A. G., et al. , 2001, ApJ, 560, 49
- Sarbu N., Rusin D., Ma C.-P., 2001, ApJ, 561, L147
- Schuecker P., Caldwell R. R., Böhringer H., Collins C. A., Guzzo L., Weinberg N. N., 2003, A&A, 402, 53
- Seljak U., 2002, MNRAS, 337, 769
- Seljak U., Zaldarriaga M., 1999, ApJ, 469, 437
- Sheth R. K., Tormen G., 1999, MNRAS, 308, 119
- Silveira V., Waga I., 1994, Phys. Rev. D, 50, 4890
- Somerville R. S., Bullock J. S., Livio M., 2003, ApJ, 593, 616
- Spergel D. N., et al. , 2003, ApJS, 148, 175
- Springel V., Yoshida N., White S. D. M., 2001, New Astronomy, 6, 51
- Swaters R. A., 1999, PhD Thesis, University of Gröningen
- Swaters R. A., Madore B. F., van den Bosch F. C., Balcells M., 2003, ApJ, 583, 732
- Tegmark M. et al., 2003a, Phys. Rev. D, in print (pre-print: astro-ph/0310723)
- Tegmark M. et al., 2003b, ApJ, submitted (preprint:astro-ph/0310725)
- Tsitsiomi A., Kravtsov A. V., Gottloeber S., Klypin A. A., 2003, ApJ, submitted (preprint:astro-ph/0311062)
- Wang L., Steinhardt P. J., 1998, ApJ, 508, 483
- Wechsler R. H., Bullock J. S., Primack J. R., Kravtsov A. V., Dekel A., 2002, ApJ, 568, 52 (W02)
- Weinberg N. N., Kamionkowski M., 2003, MNRAS, 341, 251
- Zentner A. R., Bullock J. S., 2002, Phys. Rev. D, 66, 043003
- Zentner A. R., Bullock J. S., 2003, ApJ, 598, 49
- Zhao D. H., Jing Y. P., Mo H. J., Börner G., 2003, ApJ, 597, L9